 DOI: 10.1109/JSEN.2014.2307572

Characterization of Electrical Capacitance Tomography Sensors with Different Diameter

Jiamin Ye, *Member, IEEE*, Haigang Wang, *Member, IEEE*, and Wuqiang Yang, *Fellow, IEEE*

***Abstract*—In electrical capacitance tomography (ECT), the excitation frequency and voltage, the number of excitation electrode(s), the capacitance normalization model, and the measurement strategy can be chosen. The aim of this research is to investigate their effect on ECT sensors with different diameter to improve the image quality and stability. Experimental studies have been carried out to understand the effect. Using the linear back projection algorithm, images are reconstructed for six typical permittivity distributions, and the concentration is calculated based on the reconstructed images. Preliminary conclusions are given based on the experimental results.**

***Index Terms*—Electrical capacitance tomography, sensor diameter, experimental study, numerical simulation.**

I. Introduction

As a visualization technique, electrical capacitance tomography (ECT) has been widely used for monitoring/measuring gas-solids two-phase flows, e.g. in fluidized beds, due to the advantages of its fast imaging speed, being non-intrusive and non-invasive, withstanding high temperature and high pressure and low cost [1]-[5].

The structure and performance of ECT sensors play an important role for image reconstruction. Yang addressed the key issues to optimize the design of ECT sensors, including the number and length of electrodes, the use of external and internal electrodes, implications of wall thickness and earthed screens [5]. Peng *et al*. analyzed the effect of the number of electrodes in ECT sensors on image quality and concluded that 12-electrode ECT sensors are recommended for most applications [6]. To improve the image quality for a square-shape circulating fluidized bed (CFB), Liu *et al*. presented a square ECT sensor with internal-external electrodes (IEEs) [7]. Rezvanpour *et al*. recently designed an ECT sensor with circular IEEs to investigate the droplet distribution in electrohydrodynamic atomization [8]. Ye *et al*. reported an ECT sensor of concentric annulus shape with IEEs and analyzed the performance of the sensor by numerical simulation and experiment [9] [10]. Du *et al*. studied the dynamic behavior of three gas-solids fluidized beds, 5 cm, 10 cm and 30 cm in diameter, using ECT [11]. Wang and Yang applied ECT in pharmaceutical fluidized beds and scaled up the application of ECT from a lab-scale fluidized bed to a production-scale fluidized bed [12]. Grudzień *et al*. designed an 8-electrode ECT sensor with an inner diameter of 68 cm to measure the concentration of bulk materials during gravitational flow [13].

While some previous publications discussed the application of ECT sensors with different diameter, the effect of sensor diameter on the performance of ECT sensors has not been systematically studied. The objective of this work is to investigate the image quality of ECT sensors, including the reconstructed images and the solids concentration with the increase in the diameter of ECT sensors and the number of excitation electrodes. Besides, the impact of the excitation frequency and voltage on the image quality of ECT sensors is also studied.

II. Experiment Arrangement

A. ECT sensor and measurement system

To investigate the influence of sensor diameter on the image quality of ECT, three 12-electrode ECT sensors are designed according to the conclusion of [6]. The diameter of the ECT sensors is 11 cm, 22 cm and 30 cm, respectively. Fig. 1 shows the model of the 12-electrode ECT sensors used. The covering ratio of electrodes is 90% and the height of electrodes is 5 cm. An ACECT system with 16 channels from ECT Instruments Ltd, Manchester, UK, is employed for experiment. Fig. 2 shows the measurement system and the constructed ECT sensors. To maximize the signal-to-noise ratio (SNR) of the hardware system, the frequency of the excitation signal was changed between 100 kHz and 180 kHz while the amplitude between 8 Vp-p and 24 Vp-p. Quartz sand was used for calibration. Six permittivity distributions were used for experiment, as shown in Fig. 3.

Manuscript received xx, xx, xxxx. This work was supported by the National Natural Science Foundation of China under Grant 61072001.

J. Ye and H. Wang are with the Institute of Engineering Thermophysics, Chinese Academy of Sciences, Beijing 100190, China. (e-mail: yejiamin@iet.cn; wanghaig@iet.cn)

W. Yang is with the School of Electrical and Electronic Engineering, The University of Manchester, Manchester, M13 9PL, UK. (e-mail: w.yang@manchester.ac.uk)

B. Measurement strategy

Fig. 1 (a) shows the conventional measurement strategy of one-electrode excitation. With this conventional approach, one of the electrodes is selected in turn as the excitation electrode and the others are as detection electrodes to obtain the capacitance measurements between different electrode pairs. The total number of independent capacitance measurements is

$$M = N \cdot (N-1)/2, \tag{1}$$

where N is the number of electrodes. If N = 12 then M = 66.

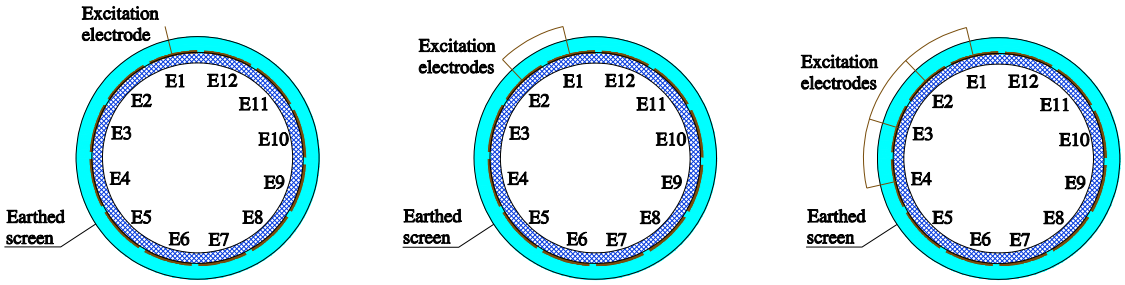

(a) (b) (c)

Fig. 1 12-electrode ECT sensors with different measurement strategies.
(a) One-electrode excitation (1E). (b) Two-electrode excitation (2E). (c) Four-electrode excitation (4E).

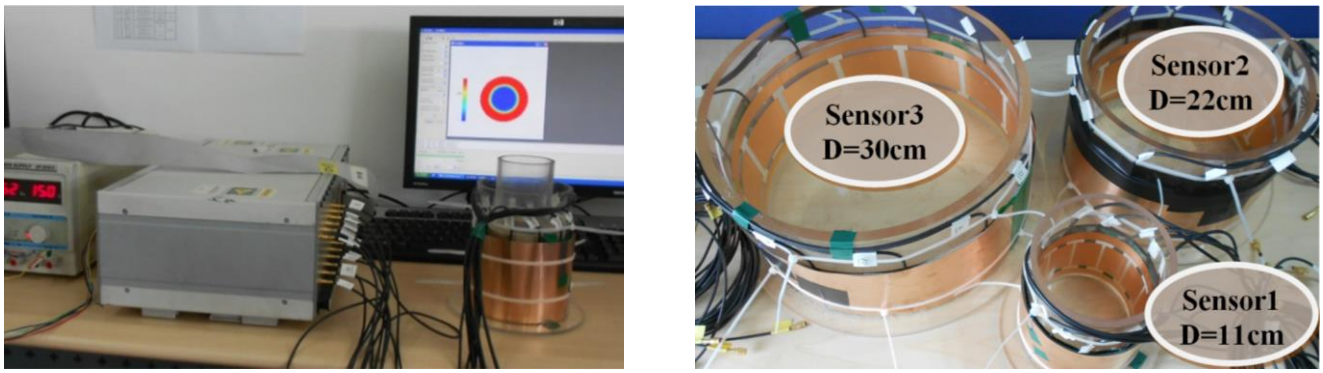

(a) (b)

Fig. 2 ACECT system and three ECT sensors. (a) ACECT system. (b) ECT sensors.

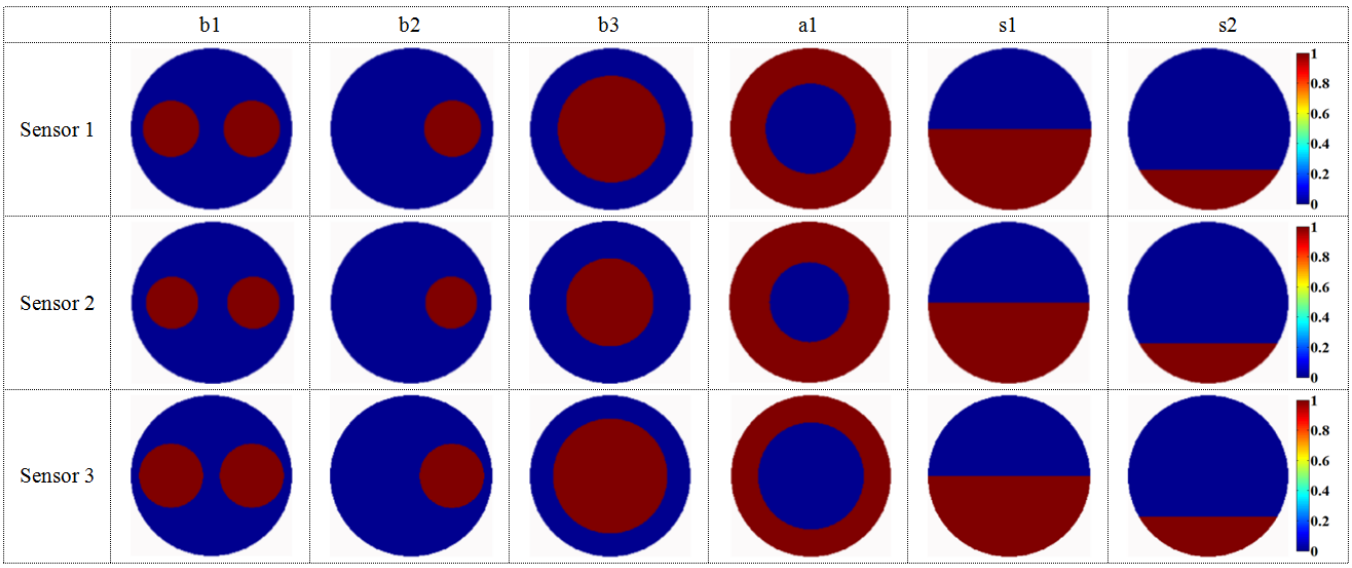

Fig. 3 Permittivity distributions for experiment.

To investigate the influence of measurement strategy on the image quality of ECT sensors of different diameter, two other measurement strategies are also applied in the experiment to compare with the one-electrode excitation, as shown in Fig. 1 (b) and (c), in which the consecutive two or four electrodes are selected as an excitation electrode array, and the other electrodes as detection electrodes. The total number of capacitance

measurements using the combined-electrode measurement strategies is

$$M = N \cdot (N - N_E), \tag{2}$$

where N_E is the number of electrodes constituted the excitation electrode array. For this work, the number of capacitance measurements is 120 and 96 respectively for the measurement strategy with 2-electrode excitation (2E) and 4-electrode excitation (4E), respectively. Note that the number of independent capacitance measurements with a 12-electrode ECT sensor is limited to 66.

C. *Normalization models*

Four normalization models, i.e. the parallel model, series model, Maxwell model [14] and Böttcher model [15], are examined in this work. These models can be expressed in (3) to (6).

$$\text{Parallel model: } C_{NP} = \frac{C_M - C_L}{C_H - C_L}, \tag{3}$$

$$\text{Series model: } C_{NS} = \frac{\frac{1}{C_M} - \frac{1}{C_L}}{\frac{1}{C_H} - \frac{1}{C_L}} = \frac{k \cdot C_{NP}}{1 + C_{NP}(k-1)}, \tag{4}$$

$$\text{Maxwell model: } C_{NM} = \frac{C_{NP} \cdot (2+k)}{3 + C_{NP} \cdot (k-1)}, \tag{5}$$

$$\text{Böttcher model: } C_{NB} = \frac{k \cdot C_{NP}}{3 \cdot C_{NP} \cdot (k-1) + 3} + \frac{2}{3} \cdot C_{NP}, \tag{6}$$

where C_M is the measured capacitance, k is the ratio of C_H and C_L, and C_H and C_L are the capacitances when the sensor is completely filled with a high-permittivity material (quartz sand in this study) and a low-permittivity material (air in this study), respectively.

III. Experimental Results and Discussion

As mentioned in [16], for different ECT sensors and different permittivity distributions, it is difficult to determine the number of iterations and the regularization parameter in some iterative algorithms and regularization algorithms. For the comparison purpose, the same algorithm, LBP [17], is used throughout this work to keep the same criterion. Using experimental data the performance of the ECT sensors of different diameter is compared.

A. *Influence of excitation frequency and voltage on the image quality*

SNR of raw data

SNR is introduced to evaluate the quality of the raw data measured from an ACECT system. Hu and Yang [18] defined SNR in an ECT system for the measured capacitance as

$$\text{SNR} = 20\log_{10}\left(\frac{\text{Signal}}{\text{Noise}}\right) = 20\log_{10}\sqrt{\frac{\sum_{i=1}^{N_F} C_{Mi}^2}{\sum_{i=1}^{N_F}\left(C_{Mi} - \overline{C_M}\right)^2}}, \tag{7}$$

where, N_F is the number of measurement frames, C_M is the measured capacitance from an electrode pair and $\overline{C_M}$ is the average of measured capacitances.

Fig. 4 shows the SNRs of the ECT sensors in Fig. 2 with different measurement strategies and different excitation strategies. The frequency of the excitation signal is changed between 100 kHz and 180 kHz while the amplitude between 8 Vp-p and 24 Vp-p. Overall, the SNR is increased with the increase in excitation frequency and excitation voltage in most cases.

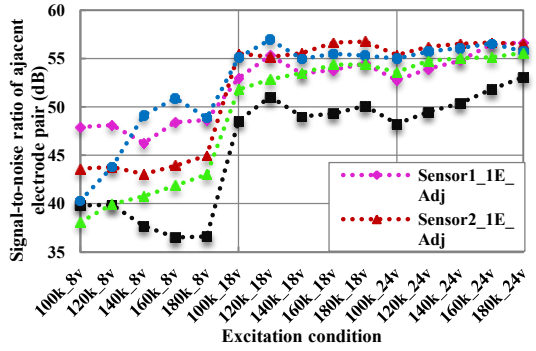

(a)

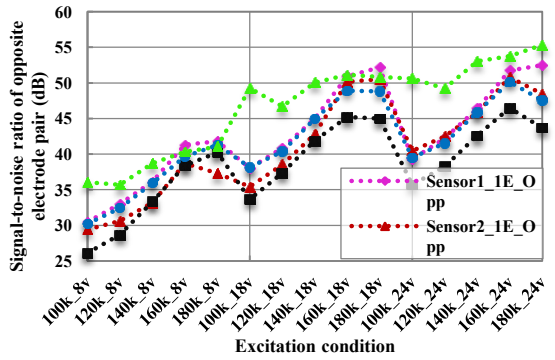

(b)

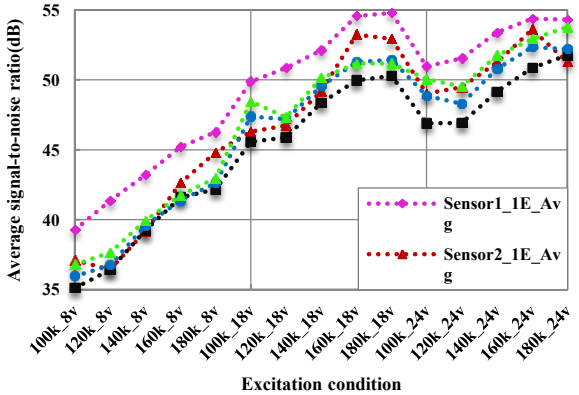

(c)

Fig. 4 SNR with different excitation strategies. (a) Adjacent electrode pair. (b) Opposite electrode pair. (c) Average value.

For the adjacent electrode pair, Sensor 3 with one-electrode excitation has the lowest SNR with all excitation strategies. With the increase in the number of excitation electrodes, the SNR is increased. Specifically, the SNR with two-electrode excitation is higher than those with four-electrode excitation. Regarding the sensors with a smaller diameter, the SNR of Sensor 1 is higher than Sensor 2 while the excitation voltage is 8 Vp-p.

For the opposite electrode pair, the data obtained from Sensor 3 also has the lowest SNR in most cases. The highest SNR is obtained from Sensor 3 with four-electrode excitation. The other curves show a similar trend.

For the average values of SNR for all electrode pairs, they are decreased with the increase in sensor diameter. The increase in the number of excitation electrode(s) can improve the SNR, but it is still worse than those from the sensor with a smaller diameter in most cases.

1) Stability of solids concentration measurement

The stability of solids concentration measurement is defined in terms of the relative standard deviation of the solids concentration as

$$\varphi_{rs} = \frac{\varphi_{std}}{\varphi_{avg}} \times 100\% , \qquad (8)$$

where φ_{std} and φ_{avg} are the standard deviation and the average value of the solids concentration of all frames, respectively.

Fig. 5 shows the relative standard deviation of the solids concentration for the permittivity distributions used for comparative studies. In addition, the average Noise/Signal for all electrode pairs defined in (7) is also introduced to compare with the variation tendency of the relative standard deviation of solids concentration. It should be note that the Noise/Signal is used for comparative study rather than SNR because the SNR has an opposite trend to the relative standard deviation of solids concentration.

In Fig. 5, it can be seen that the relative standard deviation of the solids concentration for the permittivity distributions of b1, b2 and b3 is higher than those for the permittivity distributions of a1, s1 and s2. The variation in Noise/Signal is similar to those of the relative standard deviation of the solids concentration for the three ECT sensors with different diameter and the measurement strategies with different excitation electrodes. The relative standard deviation of the solids concentration is decreased with the increase in excitation frequency and excitation voltage. In general, the excitation signal with 180 kHz and 24 Vp-p gives the most stable solids concentration. Moreover, the average Noise/Signal (or SNR) of all electrode pairs is an effective approach to evaluating the stability of the solids concentration. The lower the average Noise/Signal or the higher the average SNR, the more stable the solids concentration.

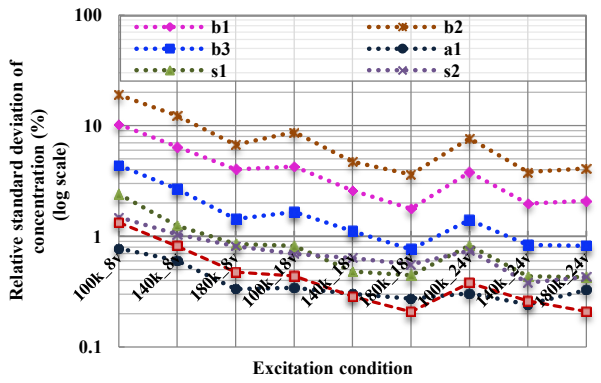

(a)

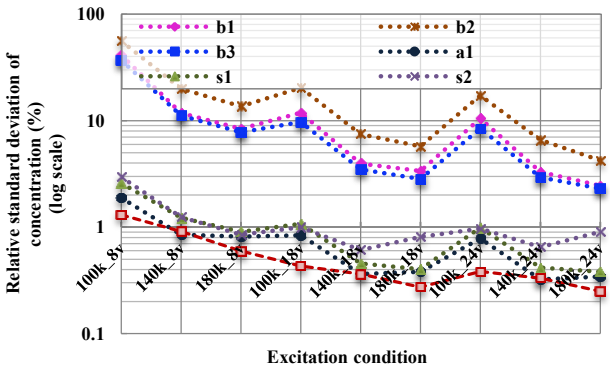

(b)

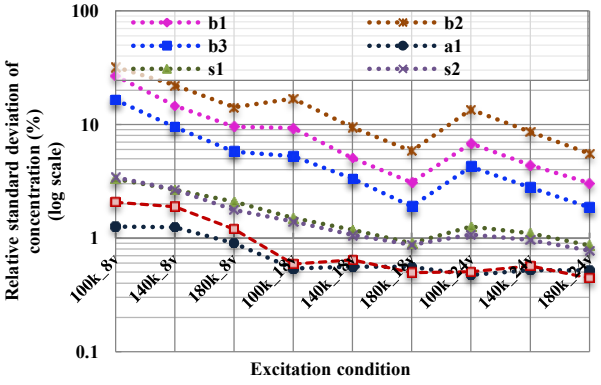

(c)

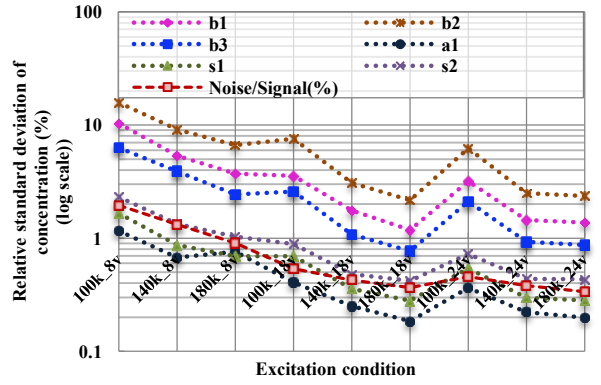

(d)

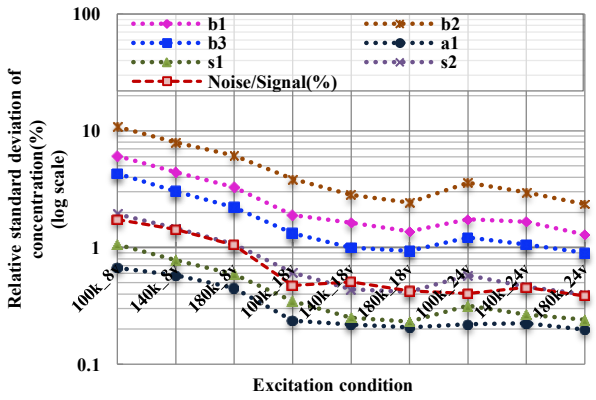

(e)

Fig. 5 Relative standard deviation of solids concentration and Noise/signal from the ECT sensors with different diameters and different measurement strategies. (a) Sensor 1 with one-electrode excitation (1E). (b) Sensor 2 with one-electrode excitation (1E). (c) Sensor 3 with one-electrode excitation (1E). (d) Sensor 3 with two-electrode excitation (2E). (e) Sensor 3 with four-electrode excitation (4E).

2) Image quality

Fig. 6 shows the images reconstructed for the permittivity distribution of b1 with the parallel model. Two excitation strategies with different frequency and different voltage are applied for comparison.

In Fig. 6 it can be seen that for all three ECT sensors, the stability and quality of the images with the excitation of 180 kHz and 24 Vp-p is dramatically better than those with the excitation of 100 kHz and 8 Vp-p. Using the excitation of 100 kHz and 8 Vp-p, the image stability and quality is obviously decreased when the sensor diameter changes from 11 cm to 22 cm or 30 cm. Furthermore, the two- or four-electrode excitation can improve the image stability compared with the one-electrode excitation.

B. Image quality of ECT sensors with exaction of 180 kHz and 24 Vp-p

In this section, only the excitation of 180 kHz and 24 Vp-p is considered to analyze the key issues in increasing the diameter of ECT sensors except for the excitation frequency and voltage.

1) Reconstructed images

Fig. 7 shows the true permittivity distributions used in Test 1 and the images reconstructed from Sensor 1 with different normalization models, i.e. the parallel model, series model, Maxwell model and Böttcher model. In Fig. 7, it can be seen that the images reconstructed for the permittivity distributions of b3, a1, s1 and s2 are similar to each other regardless of the normalization models. For the permittivity distributions of b1 and b2, the profile of the images reconstructed with different normalization models have no obvious difference. It is important to note that the images reconstructed with the series model have the closest permittivity value to the true permittivity. It implies that the series model is applicable in the situation where the high-permittivity material is present in dilute quantities in the mixture [19].

Fig. 8 shows the images reconstructed from Sensor 2. Because of no significant difference between the images reconstructed with different normalization models, only the images with parallel model are shown in Fig. 8. Compared with Test 1, the sensor diameter is increased from 11 cm to 22 cm. The true permittivity distribution utilized in Test 2 is similar to those in Test 1. However, the spatial resolution of the images reconstructed from Sensor 2 for the permittivity distributions of b3, a1, s2 and s2 is significantly decreased. Moreover, the permittivity value of the images reconstructed for the permittivity distributions of b1, b2 and b3 is also decreased compared with those from Sensor 1.

Fig. 9 compares the images reconstructed from Sensor 3 using three different measurement strategies, one-electrode excitation (1E), two-electrode excitation (2E) and four-electrode excitation (4E). The parallel model is used in Test 3 to calculate the normalized capacitances.

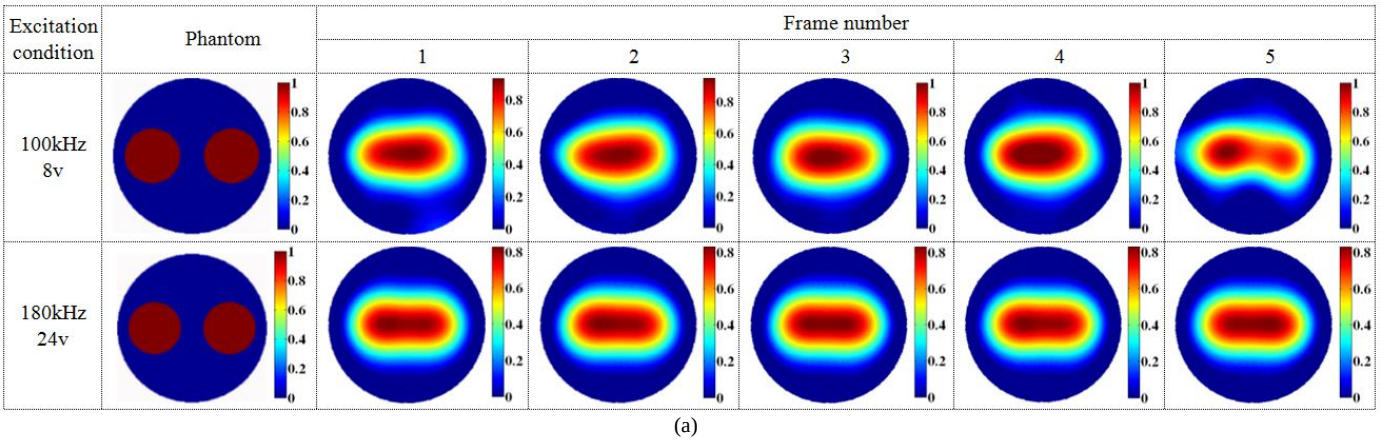

(a)

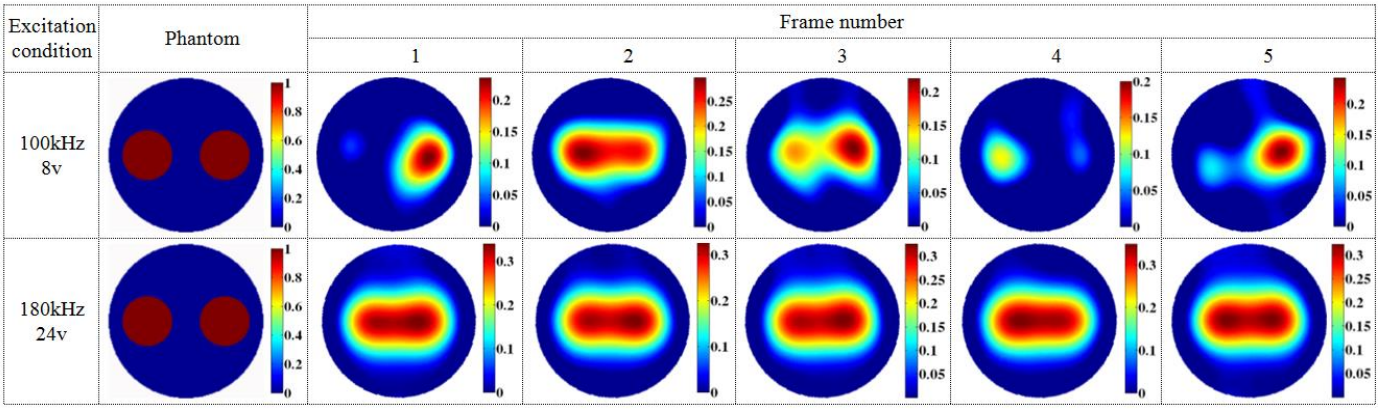

(b)

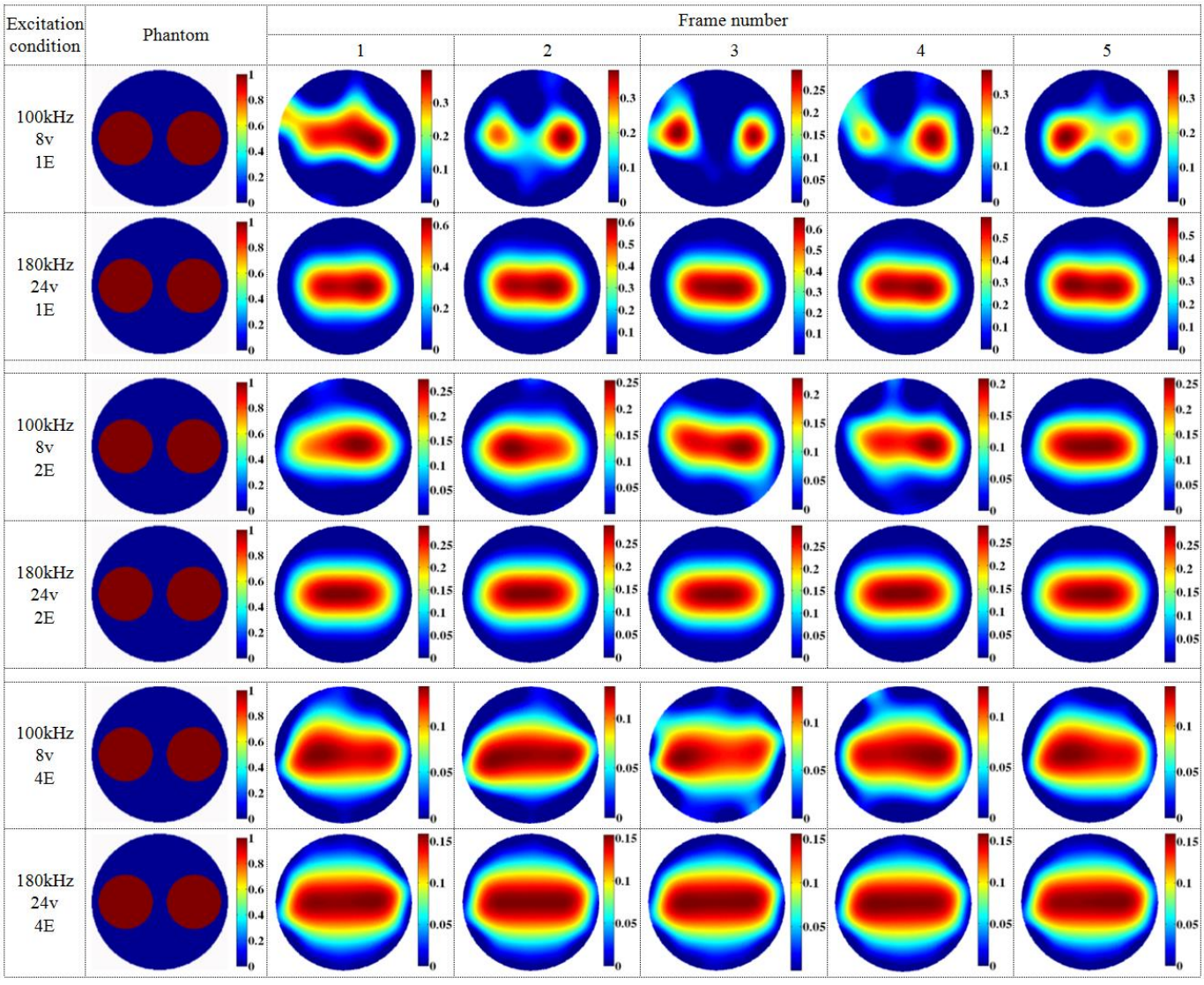

(c)

Fig. 6 Images reconstructed for the permittivity distribution of b1 with the parallel model. (a) Sensor 1. (b) Sensor 2. (c) Sensor 3.

With one-electrode excitation, the images reconstructed for the distributions of b1, b2 and b3 from Sensor 3 have a higher permittivity than those from Sensor 2. The possible reason is the true solids concentration is higher than those in Test 2. For all permittivity distributions, the image contrast and spatial resolution are similar to those from Sensor 2, but they are still not better than those from Sensor 1.

Fig. 9 also shows the images reconstructed from Sensor 3 with two-electrode excitation. Compared to the images reconstructed from Sensor 3 with one-electrode excitation, the im-

ages reconstructed with two-electrode excitation have a lower spatial resolution for almost all permittivity distributions. It is worth noting that the profile of the images reconstructed for the permittivity distributions of s1 and s2 with two-electrode excitation is closer to the true permittivity distributions than those with one-electrode excitation.

The spatial resolution of the images reconstructed from Sensor 3 with four-electrode excitation is decreased obviously compared with the images reconstructed from Sensor 3 with two-electrode excitation. For the permittivity distributions of a1, s1 and s2, the solids concentration near the center is higher than those from Sensor 3 with one- and two-electrode excitation. In addition, the experimental results indicate that the normalization model has no significant influence on the image quality.

2) Solids concentration error

To quantitatively compare the image quality of the ECT sensors with different diameter, the solids concentration is calculated based on the reconstructed images. Fig. 10 shows the solids concentration for six typical permittivity distributions with four normalization models. The relative solids concentration can be calculated as

$$\varphi_{re} = \frac{(\hat{\varphi} - \varphi)}{\varphi} \times 100\%, \tag{9}$$

where φ is the true solids concentration for one frame and $\hat{\varphi}$ is the estimated solids concentration.

Fig. 10 (a), (b) and (c) show the calculated solids concentration with one-electrode excitation. In Fig. 10 (a), (b) and (c), it can be seen that the solids concentration for the permittivity distributions of b1, b2 and b3 is significantly decreased with the increase in sensor diameter compared with the true concentration. Specifically, the solids concentration calculated from Sensor 1 for the permittivity distributions of b1 and b2 is very close to the true concentration. In contrast, the solids concentration for the permittivity distributions of a1, s1 and s2 is increased with the increase in sensor diameter. This phenomenon can be seen when the sensor diameter changes from 11 cm to 22 cm. For the permittivity distributions of a1 and s2, the concentration calculated from Sensor 2 and Sensor 3 is nearly the same as the true concentration.

Fig. 10 (d) and (e) show the solids concentration calculated from Sensor 3 with two- and four-electrode excitation, respectively. Compared with Fig. 10 (c), the solids concentration error for the permittivity distributions of b1, b2 and b3 in Fig. 10 (d) and (e) is decreased. In contrast, the solids concentration error for the permittivity distribution of a1, s1 and s2 is increased with the increase in the number of excitation electrode.

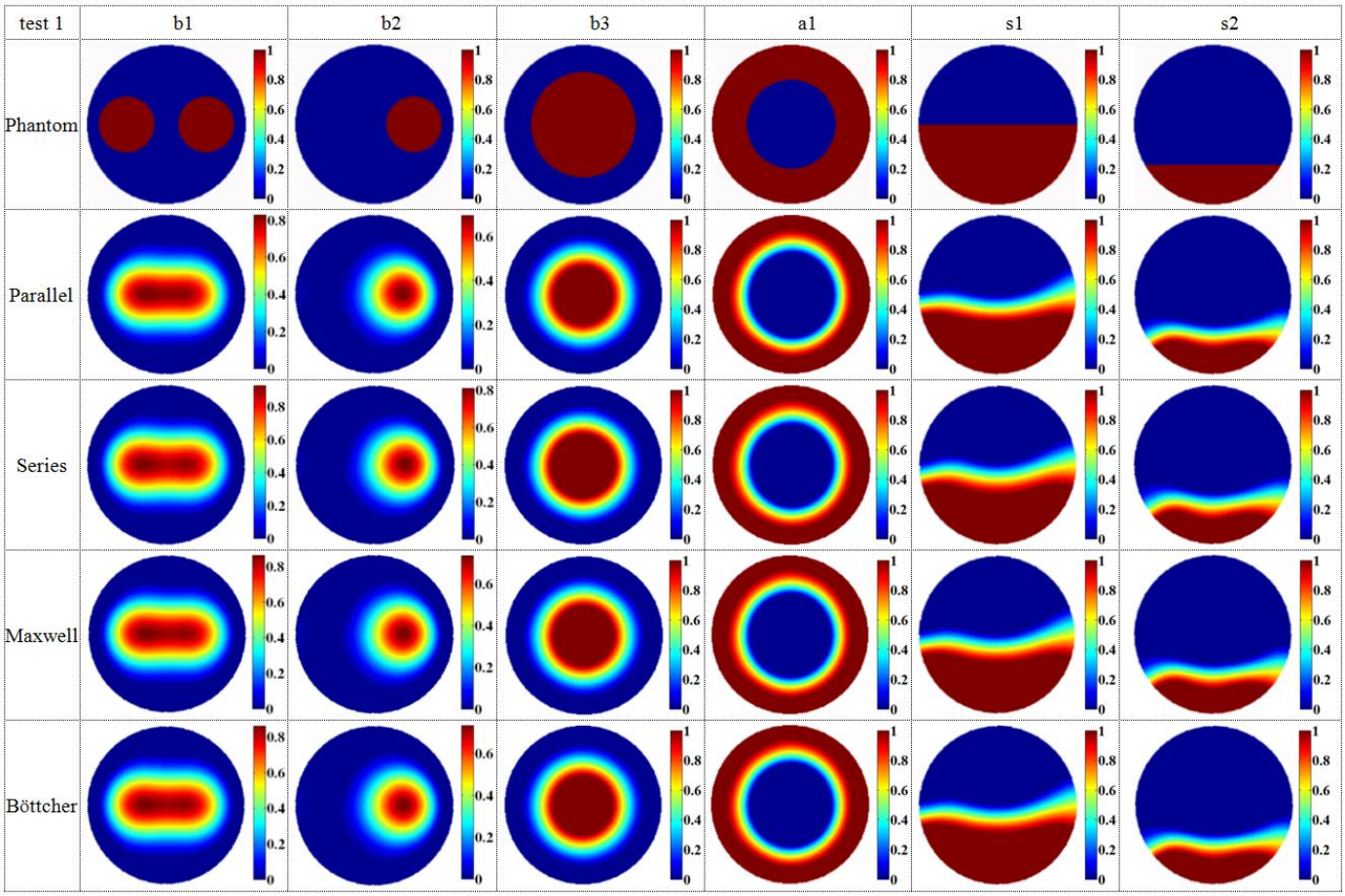

Fig. 7 Images reconstructed from Sensor 1 with one-electrode excitation of 180 kHz and 24 Vp-p.

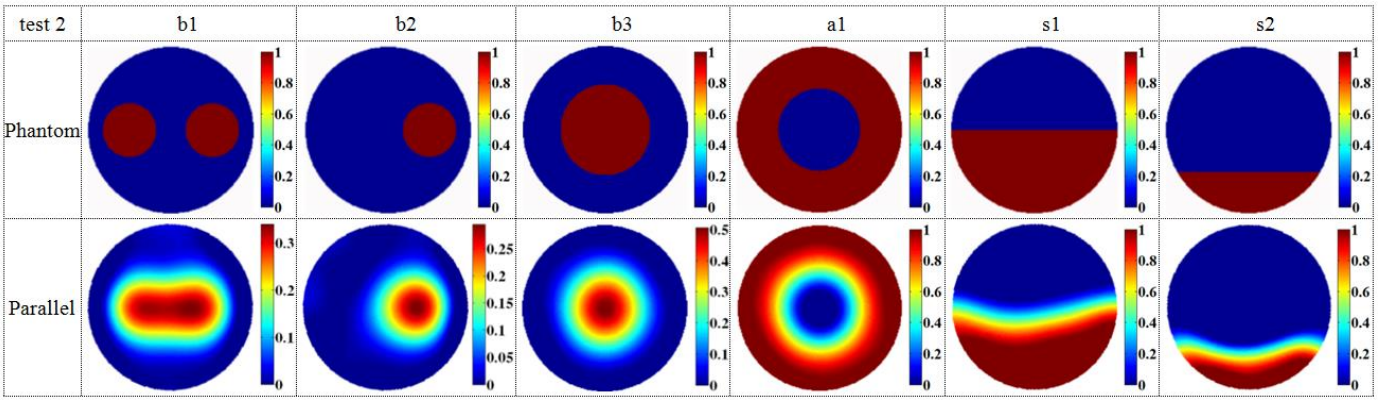

Fig. 8 Images reconstructed from Sensor 2 with one-electrode excitation of 180 kHz and 24 Vp-p.

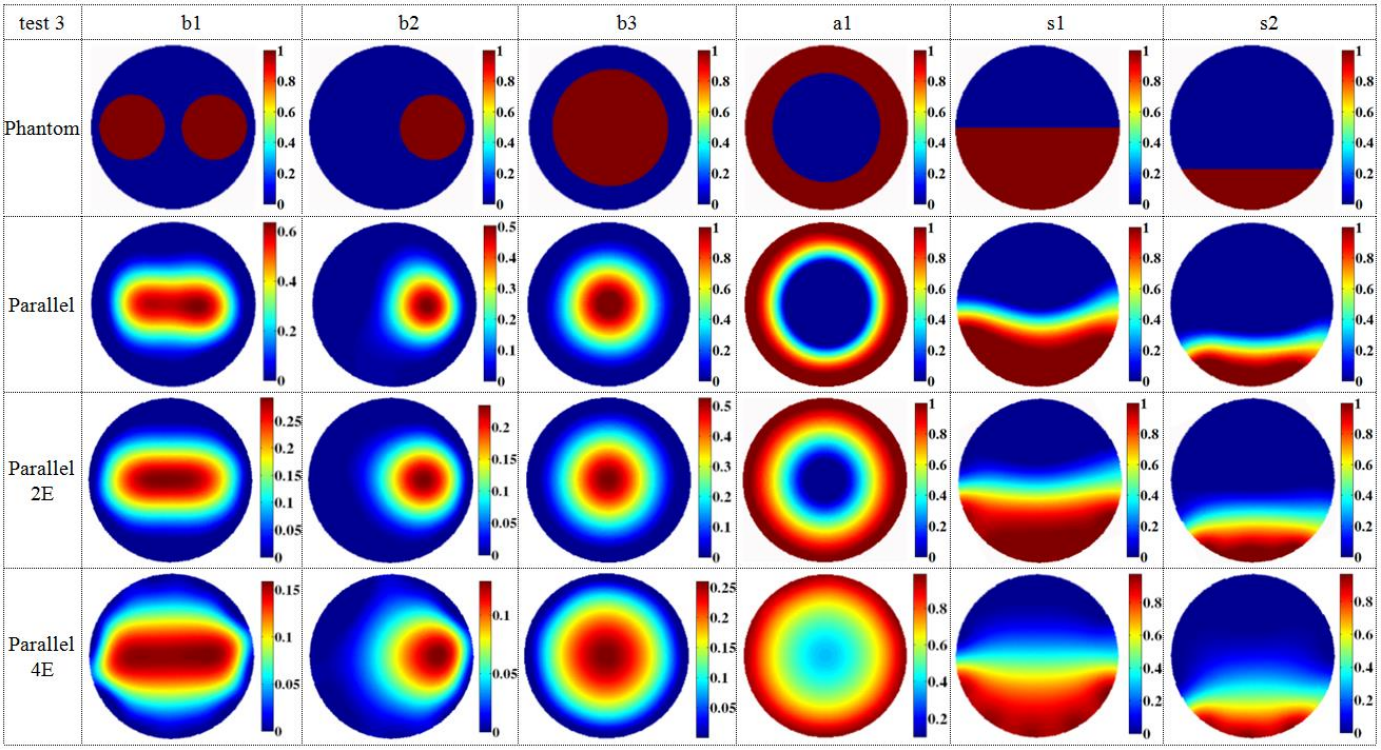

Fig. 9 Images reconstructed from Sensor 3 with different excitation strategies of 180 kHz and 24 Vp-p.

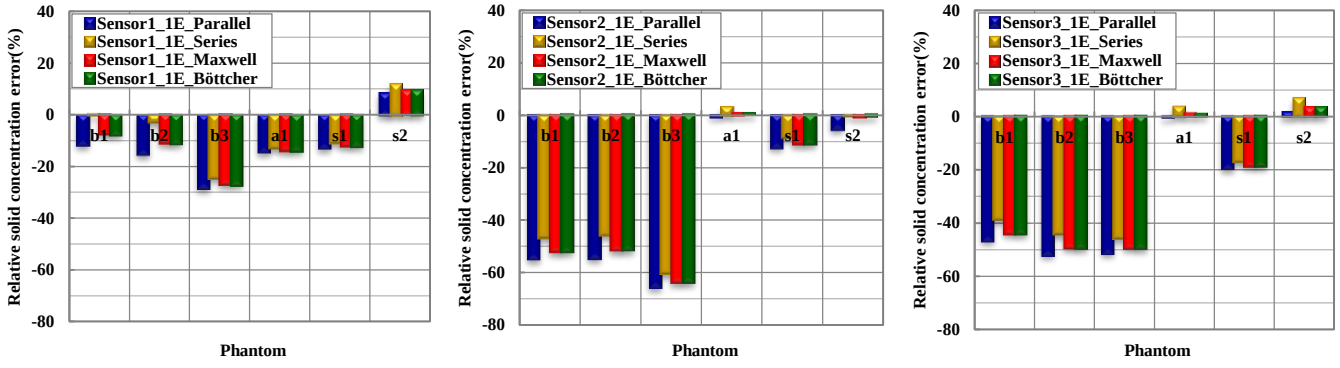

(a) (b) (c)

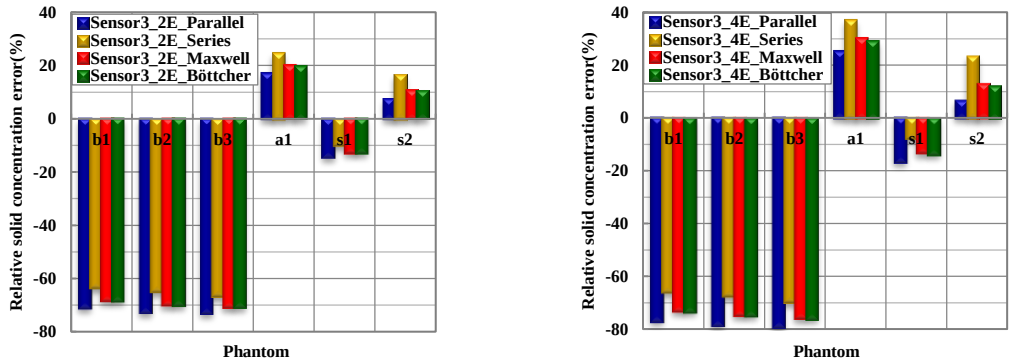

Fig. 10 Relative solids concentration error calculated from three ECT sensors using different measurement strategies with the excitation of 180 kHz and 24 Vp-p. (a) Sensor 1 with one-electrode excitation (1E). (b) Sensor 2 with one-electrode excitation (1E). (c) Sensor 3 with one-electrode excitation (1E). (d) Sensor 3 with two-electrode excitation (2E). (e) Sensor 3 with four-electrode excitation (4E).

3) Sensitivity analysis

To study the effect of increasing sensor diameter on the sensitivity map of ECT, a comparison is done with three ECT sensors of varying diameter. The sensitivity map can be defined as

$$S_{ij}(x,y) = -\iint_{p(x,y)} \frac{\nabla\phi_i(x,y)}{V_i} \cdot \frac{\nabla\phi_j(x,y)}{V_j} dxdy \,, \qquad (10)$$

where $S_{ij}(x,y)$ is the sensitivity between the *i*th electrode and the *j*th electrode over the area $p(x,y)$, $\phi_i(x,y)$ is the potential distribution inside the sensing domain while the *i*th electrode is selected as an excitation electrode with a voltage V_i applied on it and the other electrodes are used as detection electrodes.

The influence of the measurement strategies with different number of excitation electrodes on sensitivity is investigated. Fig. 11 shows the normalized sensitivity distributions between the adjacent electrode pair and opposite electrode pair. In addition, the averaged sensitivity of each pixel due to different electrode pairs is also calculated and illustrated in Fig. 11.

First of all, the effect of increasing sensor diameter is discussed. In Fig. 11, it can be seen that the sensitivity between the adjacent electrode pairs does not change obviously with the increase in sensor diameter. On the other hand, the sensitivity between the opposite electrode pairs shows some differences with the increase in sensor diameter. More specifically, the distribution of sensitivity near the central area is more dispersed when the sensor diameter changes from 11 cm to 22 cm or 30 cm. This results in the decrease in spatial resolution for most permittivity distributions with the increase in sensor diameter.

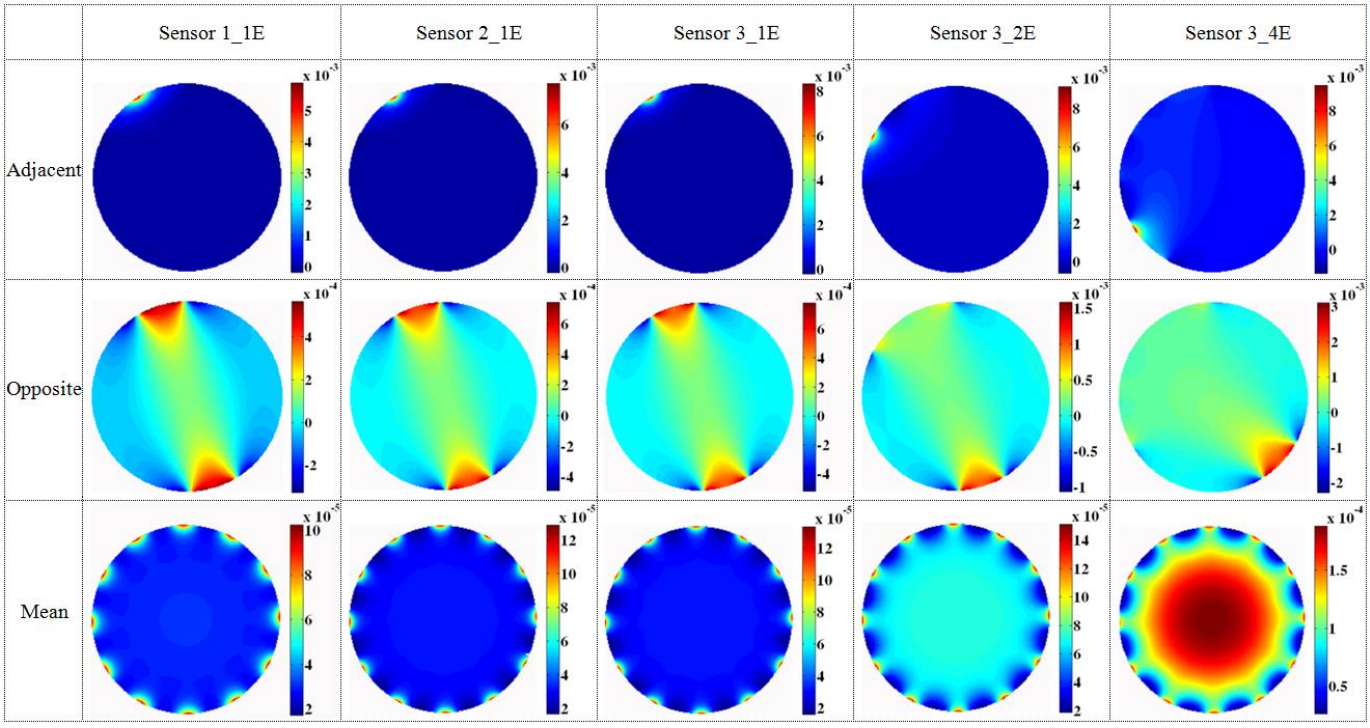

Fig. 11 Normalized sensitivity distribution with different ECT sensors and different measurement strategies.

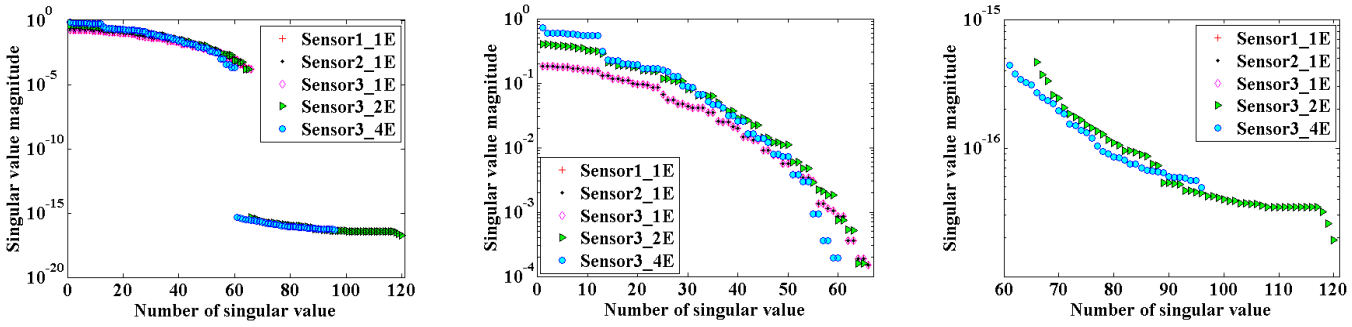

(a) (b) (c)

Fig. 12 Spectral analysis to compare the magnitude of the singular values for three ECT sensors with different measurement strategies (log scale). (a) SVD plot. (b) Details of part 1 of (a). (c) Details of part 2 of (a).

Next, the effect of measurement strategies on sensitivity distributions is investigated. Fig. 11 shows that the sensitivity distributions either between the adjacent electrode pairs or between the opposite electrode pairs are more dispersed with the increase in the number of excitation electrodes. The lower spatial resolution caused by this phenomenon can be seen in Fig. 9. Fig. 11 also demonstrates that the averaged sensitivity near the central area is decreased with the increase in the number of excitation electrodes with one-electrode excitation. This can be verified from the reconstructed images for the permittivity distributions of s1 and s2, as shown in Fig. 7, Fig. 8 and Fig. 9. The area of the second phase near the central region in the images reconstructed for the permittivity distributions of s1 and s2 is decreased with the increase in sensor diameter. Considering the measurement strategy, the sensitivity in the center is significantly increased with the increase in the number of excitation electrodes. This results in the expansion of the second phase approaching the central area in the reconstructed images, as shown in Fig. 9.

To further examine the effect of the measurement strategies and the diameter of ECT sensors, the sensitivity matrix is analyzed using singular value decomposition (SVD). As shown in Fig. 12, the singular values for Sensor 3 with two- and four-electrode excitation are effectively zero. It means that the corresponding singular vector does not contribute to the image reconstruction. Moreover, with two- and four-electrode excitation, only 65 and 60 measurements are unique, respectively. Fig. 12 (b) shows the details of part 1 of Fig. 12 (a). In Fig. 12 (b), it can be seen that the singular values from all the sensors with one-electrode excitation have almost the same magnitudes. For Sensor 3, as the number of excitation electrodes increases from one to two, the magnitudes of the singular values are increased, suggesting that the spectral components become more stable as the number of excitation electrodes increases. When the number of excitation electrodes increases to four, some magnitudes of the singular values are lower than those from Sensor 3 with one- and two-electrode excitation. It means that the stability of the measurements is decreased with four-electrode excitation.

4) Normalized capacitance

The normalized capacitances are usually utilized for the image reconstruction. Fig. 13 compares the capacitances calculated using the four different normalization models, i.e. the parallel model, series model, Maxwell model and Böttcher model. The permittivity distribution of s2 is selected as an example for comparison.

In most cases, the capacitances calculated using the parallel model and series model have the lowest and highest values, respectively. The capacitances calculated using the Maxwell model and Böttcher model are fairly similar. This explains the similarity of images shown in Fig. 7.

For all distributions, the normalized capacitances calculated from the sensors with different diameters and different measurement strategies have generally similar distributions. However, the magnitude of the normalized capacitances is not exactly the same. Especially, the highest values of the normalized capacitances are decreased when the sensor diameter changes from 11 cm to 22 cm. For Sensor 2 and Sensor 3, the highest values of the normalized capacitances have no obvious difference. Regarding the measurement strategy, the highest value of the normalized capacitances has a slightly decrease with the increase in the number of excitation electrodes.

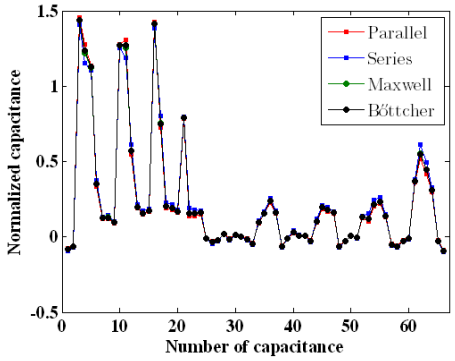

(a)

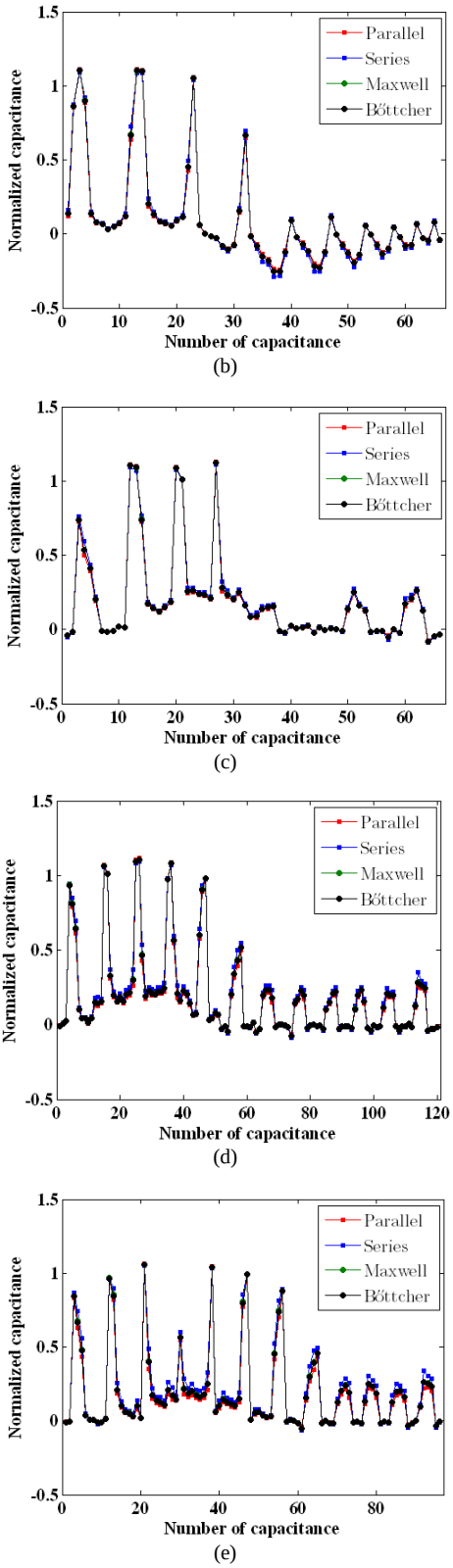

Fig. 13 Normalized capacitance distribution for permittivity distribution of s2 with the excitations of 180 kHz and 24 Vp-p. (a) Sensor 1 with one-electrode excitation (1E). (b) Sensor 2 with one-electrode excitation (1E). (c) Sensor 3 with one-electrode excitation (1E). (d) Sensor 3 with two-electrode excitation (2E). (e) Sensor 3 with four-electrode excitation (4E).

IV. Conclusions

By considering the influence of the excitation frequency and voltage, the sensor diameter, the measurement strategy and the capacitance normalization model, the issues with the increase in diameter of ECT sensors are discussed based on experimental data.

In general, the SNR of the raw data is increased with the increase in excitation voltage and excitation frequency. The average SNR for all electrode pairs is decreased with the increase in sensor diameter. Compared with the one-electrode excitation, the measurement strategy with two- and four-electrode excitation can improve the SNR. Moreover, the SVD analysis on sensitivity matrix concluded that the measurement strategy with two-electrode excitation can obtain more stable measurements.

With one-electrode excitation, the image contrast for the distributions with high permittivity in the central area is decreased when the diameter of ECT sensors changes from 11 cm to 22 cm or 30 cm. On the other hand, the image contrast for the distributions with high permittivity in the near-wall region has no obvious difference as the sensor diameter increases. However, the spatial resolution of the images is decreased as the sensor diameter changes from 11 cm to 22 cm or 30 cm.

The increased number of excitation electrode results in the increase in the permittivity of reconstructed images in the central area. Furthermore, the spatial resolution of the reconstructed images is decreased regardless of the permittivity distribution with the increase in the number of excitation electrodes.

The relative solids concentration error for the true distributions with high permittivity in the central area is increased with the increase in sensor diameter. In contrast, the relative solids concentration error for the true distributions with high permittivity in the near-wall region is decreased with the increase in sensor diameter in most cases. The increase in the number of excitation electrode can increase the relative solids concentration error.

The sensor diameter has almost no effect on the normalized sensitivity. With the increase in the number of excitation electrode, the sensitivity is enhanced, especially in the central area. The normalized capacitances are decreased when the sensor diameter changes from 11 cm to 22 cm or 30 cm, regardless of the permittivity distributions. The normalized capacitances decrease with the increase in the number of excitation electrode(s). The normalization model has no obvious influence on the normalized capacitances and the reconstructed images.

References

[1] Y. T. Makkawi and P. C. Wright, "Fluidization regimes in a conventional fluidized bed characterized by means of electrical capacitance tomography," *Chem. Eng. Sci.*, vol.57, no.13, pp.2411-2437, 2002.

[2] S. Liu, Q. Chen, H.G. Wang, F. Jiang, I. Ismail and W. Q. Yang, "Electrical capacitance tomography for gas-solids flow measurement for circulating fluidized beds," *Flow Meas. Instrum.*, vol.16, no.2, pp.135-144, 2005.

[3] C. Wang, Z. Lv and D. Li, "Experimental study on gas–solids flows in a circulating fluidised bed using electrical capacitance tomography," *Powder Technol.*, vol.185, no.2, pp.144-151, 2008.

[4] H.G. Wang, W.Q. Yang, P. Senior, R.S. Raghavan and S.R. Duncan, "Investigation of batch fluidized-bed drying by mathematical modeling, CFD simulation and ECT measurement," *AIChE J.*, vol.54, no.2, pp.427-444, 2008.
[5] W.Q. Yang, "Design of electrical capacitance tomography sensors," *Meas. Sci. Technol.*, vol.21, no.4, 042001, 2010.
[6] L.H. Peng, J.M. Ye, G. Lu and W.Q. Yang, "Evaluation of effect of number of electrodes in ECT sensors on image quality," *Sensors Journal, IEEE*, vol.12, no.5, pp.1554-1565, 2012.
[7] S. Liu, W. Q. Yang and H.G. Wang, "An electrical capacitance tomography sensor with internal-external electrodes," *Proc. SPIE*, vol.4188, pp. 300-307, 2001.
[8] A. Rezvanpour, C. Wang, Y. Liang and W.Q. Yang, "Investigation of droplet distribution in electrohydrodynamic atomization (EHDA) using an AC-based electrical capacitance tomography (ECT) system with an internal–external electrode sensor," *Meas. Sci. Technol.*, vol.23, no.1, 015301, 2012.
[9] J.M. Ye, W.Q. Yang, "Evaluation of Electrical Capacitance Tomography Sensors for Concentric Annulus," *Sensors Journal, IEEE*, vol.13, no.2, pp.446-456, 2013.
[10] J.M. Ye, Y. Li, H.G. Wang, R.H. Ge, and W.Q.Yang, "Concentric-annulus electrical capacitance tomography sensors," *Meas. Sci. Technol.*, vol.24, no.9, 095403, 2013.
[11] B. Du, W. Warsito and L.S. Fan, "ECT studies of gas-solid fluidized beds of different diameters," *Industrial & engineering chemistry research*, vol.44, no.14, pp.5020-5030, 2005.
[12] H.G. Wang and W.Q. Yang, "Scale-up of an electrical capacitance tomography sensor for imaging pharmaceutical fluidized beds and validation by computational fluid dynamics," *Meas. Sci. Technol.*, vol.22, no.10, 104015, 2011.
[13] K. Grudzień, Z. Chaniecki, B. Matusiak, A. Romanowski, G. Rybak and D. Sankowski, "Visualisation of Granular Material Concentration Changes, During Silo Discharging Process, Using ECT Large Scale Sensor," *Image Processing & Communications*, vol.17, no.4, pp.327-338, 2012
[14] T.R. McKeen and T.S. Pugsley, "The influence of permittivity models on phantom images obtained from electrical capacitance tomography," *Meas. Sci. Technol.*, vol.13, no.12, pp.1822-1830, 2002.
[15] M. Louge and M. Opie, "Measurements of the effective dielectric permittivity of suspensions," *Powder Technol.*, vol.62, no.1, pp.85-94, 1990.
[16] S. Liu, H.G. Wang, F. Jiang and W. Q. Yang, "A new image reconstruction method for tomographic investigation of fluidized beds," *AIChE J.*, vol.48, no.8, pp.1631-1638, 2002.
[17] W.Q. Yang and L.H. Peng, "Image reconstruction algorithms for electrical capacitance tomography," *Meas. Sci. Technol*., vol.14, no.1, R1, 2003.
[18] X.H. Hu and W.Q. Yang, "Design of a data acquisition and function generation unit with USB," *Meas. Sci. Technol.* vol.17, no.4, N17–23, 2006.
[19] Process Tomography Ltd, "Calculation of volume ratio for ECT sensors," *PTL Application Note AN2*.

Jiamin Ye (M'12**)** received the BEng, MSc and PhD degrees in control science and engineering from Tianjin University, Tianjin, China, in 2004, 2006 and 2009, respectively.

She is currently an Associate Professor with the Institute of Engineering Thermophysics, Chinese Academy of Sciences, Beijing, China. Her current research interests include industrial process tomography, image reconstruction, instrumentation and multiphase flow measurement.

Haigang Wang (M'09) received the BEng degree from Harbin Engineering University, Harbin, China, in 1996, the MSc degree from Dalian University of Technology, Dalian, China, in 1999 and the PhD degree from the Institute of Thermophysics Engineering, Chinese Academy of Sciences, Beijing, China, in 2003.

He is currently a Professor with the Institute of Engineering Thermophysics, Chinese Academy of Sciences, Beijing, China. His research interests include measurement and simulation of multiphase flow, process tomography and 3D graphics software development.

Wuqiang Yang (SM'05, F'12) received all his degrees, BEng (Distinction) 1982, MSc 1985 and PhD (Distinction) 1988, from Tsinghua University, Beijing, China. After three years as a Lecturer with Tsinghua University, he joined the University of Manchester Institute of Science and Technology (now The University of Manchester), Manchester, U.K., in 1991, where he is currently a Professor. He is a Visiting Professor with six universities, and has been invited by many universities, research institutions and international conferences worldwide to give lectures, seminars, and keynotes. He has published 300 papers and holds ten patents. His current research interests include electrical capacitance tomography.

Dr. Yang is an Editorial Board Member/Associate Editor of six journals, a Guest Editor of several journal special issues, and reviews papers for 40 professional journals, including six IEEE Transactions. Since 2002, his biography has been in Who's Who in the World. He is currently the IEEE Instrumentation and Measurement Society Distinguished Lecturer.